ta-C deposition simulations: Film properties and time-resolved dynamics of film formation

H. U. Jäger* and A. Yu. Belov†

Forschungszentrum Rossendorf e.V., Institut für Ionenstrahlphysik und Materialforschung, Postfach 510119, 01314 Dresden, Germany

(Received 17 October 2002; revised manuscript received 24 March 2003; published 9 July 2003)

Ion beam deposition of carbon films was studied by molecular-dynamics simulations. Using an analytic hydrocarbon potential of Brenner with an increased C-C interaction cutoff value, deposition of films with a thickness of up to 10 nm was simulated for ion energies $E_{ion}=10-80$ eV, and for substrate temperatures T_s ranging from 100 to 900 K. The bulk properties of the computed tetrahedral amorphous carbon (ta-C) films as well as structure and roughness of their sp^2-rich surface layers agree qualitatively with experiment. At low ion energies and low substrate temperatures, the sp^3 fraction in the films increases with ion energy, resulting in a highly sp^3-bonded ta-C with a high compressive stress for $E_{ion}>30$ eV. This trend remains also at room temperature, however with lower sp^3 content and stress. In agreement with experiment the simulations predict a sharp transition from ta-C to graphitic carbon as T_s exceeds a critical temperature T_c. The calculated value for T_c is a bit too low ($T_c\sim100$ °C for $E_{ion}=40$ eV). For the ion energies $E_{ion}\leqslant80$ eV, the incidence atom is predicted to come to rest in the sp^2-rich surface layer. A time-resolved analysis of the film formation shows that atom subplantation leads generally to a highly tetrahedral structure, but above T_c the kinetic energy of the atoms is sufficiently large to overcome the barrier in cohesive energy between ta-C and the more stable graphitelike films.

DOI: 10.1103/PhysRevB.68.024201 PACS number(s): 61.43.Bn, 68.55.−a, 68.60.Bs, 81.05.Uw

I. INTRODUCTION

The atomic network of hydrogen-free amorphous carbon films[1] consists of three- (sp^2) and fourfold coordinated (sp^3) sites. The respective fractions of these two bonding types determine the film properties, which vary from graphitelike to diamondlike as the sp^3 content increases. Films with a high content (80–90 %) of tetrahedrally coordinated atoms can be deposited by means of hyperthermal carbon ion beams with energies of typically ~20 eV-1 keV. These films have diamondlike properties and an atomically smooth surface. They are known as tetrahedral amorphous carbon (ta-C), and are expected to become significant for applications, e.g., as cathode material in field emission displays,[2] or as ultrathin coatings in magnetic storage technology.[3]

It is now widely accepted that the formation of ta-C films is due to an internal subsurface growth induced by the shallow carbon ion implantation. The deposition process was analyzed in terms of phenomenological models[4] such as the ''subplantation models'' of Lifshitz *et al.*[5] and of Robertson.[6] The film structure in these models is determined by an interplay between two processes: densification by incoming energetic ions and relaxation of density. While the ballistic part of the deposition process is now well understood, the nature of relaxation phenomena in ta-C growth still remains unclear. In particular, the strong dependence of the sp^3 content on substrate temperature T_s is not yet fully explained. The structure of films deposited from medium energy ions is known to depend critically on T_s. Deposition at room temperature produces films containing up to $\sim85\%$ of carbon atoms with sp^3 hybridization. This value remains nearly constant below a transition temperature, T_c, of ~200 °C at ion energies around 100 eV. Above T_c, it falls abruptly, indicating a transition from ta-C to graphitic carbon with dominating sp^2 bonding.

It is an attractive goal to understand the ta-C deposition process and especially its critical dependence on substrate temperature from an atomistic perspective. During the past decade, the increasing computational capabilities and the progress in developing C-C atom potentials encouraged some groups to approach the problem and to perform related molecular-dynamics (MD) investigations.[7–17] Using two-dimensional MD simulations, Marks *et al.*[9] studied the relationship between the ion-beam energy and the resultant film stress. Three-dimensional MD simulations of the deposition of unhydrogenated ta-C films were reported by Uhlmann *et al.*,[10] by Kaukonen and Nieminen,[11–13] by us,[14] by Yastrebov and Smith,[15] and quite recently by Marks.[16,17] In these calculations, the lateral dimensions of the substrate unit cells were similar in magnitude, they were about 10–20 Å. Uhlmann *et al.*[10] derived the forcefields from a density-functional (DF) based tight-binding method. The CPU time for computing an ion impact was about 100 h. Therefore, they started from an appropriately preconstructed ta-C cell and simulated the structural changes induced by an ion fluence equivalent to only one monolayer. It could be shown, in qualitative accordance to experimental data, that the evolving diamondlike carbon films are characterized by a deep sp^3-rich dense layer below a defective, low density sp^2-rich surface layer.

Deposition simulations for significantly higher fluences are feasible[11–17] if empirical C-C potentials are used. The potentials developed for covalent bonding about one decade ago follow the bond-order formalism of Abell.[18] The binding energy of the system is a sum of nearest-neighbor pair interactions moderated by the local atomic environment. The empirical potentials are computationally much more efficient than quantum mechanical methods like that of Ref. 10. But the pregiven form of the potential energy function and the fit of its parameters to a limited set of materials properties are aspects that need attention in performing classical MD deposition simulations.

The MD simulations of Kaukonen and Nieminen[11–13] were done using the empirical potential of Tersoff.[19] The

 ©2003 The American Physical Society

deposited films consisted of up to twenty atomic layers,[12] and were found to become most diamondlike when the ion energy was in the range of 40–70 eV. The maximum sp^3 fraction[11] was 44%, approximately half of the experimentally observed value. In their latest paper,[13] the authors focused upon the details of the atomic rearrangement processes induced by a single deposition event. The problem is that the sp^3 fraction computed in these investigations stems mostly from a specific term of the Tersoff potential that may be questioned.[14] The Tersoff potential overestimates the binding energy for a C-C atom pair where one carbon atom with three nearest neighbors is bonded to a carbon atom with four neighbors. This aspect was discussed by Brenner, who developed an empirical potential-energy expression for hydrocarbons,[20] introducing the so-called overbinding correction which was determined by fitting the vacancy formation energies in diamond and graphite. The Brenner potential was designed to account not only for three possible hybridizations (sp^1, sp^2, sp^3) in C, but also different types of bonding between sp^2 sites: double bonds (like in ethylene) and conjugated bonds (like in graphite).

One of the original goals of Brenner was to develop a potential which can be used in simulating the chemical vapor deposition of diamond films. The authenticity of this hydrocarbon potential to predict correctly the chemical reactions at diamond surfaces was examined in detail in a series of more accurate theoretical investigations.[21–23] For nonhydrogenated diamond (001)-(2×1) surfaces the Brenner potential predicts formation of π-bonded dimers with the same double bond length of 1.38 Å as in an ethylene molecule. The Hartree-Fock calculations[21] for small C_9H_{12} clusters representing a single dimer showed that the such dimers are described by a single σ-bond and radicals rather than by a $\sigma+\pi$ double bond. In contrast to Ref. 21, an analysis[23] employing DF theory within the local density approximation and a 64-atom supercell predicted the formation of π-bonded dimers and was consistent with the results based on the Brenner potential.

For the use in modeling film deposition by hyperthermal particles, the Brenner potential in its original form proved to be inadequate.[14,15] In the Tersoff and Brenner potentials, the range for the binding orbitals represented by the outer cutoff value[24] S is 2.1 or 2.0 Å. Interactions of longer range are not included. Such an interaction range of $\leqslant$2.1 Å is too short to describe transitions from graphite- to diamond-like carbon systems.[25,26,14]

In our ta-C deposition simulations[14] we adopted the Brenner potential[20] and modified it in a rather simple way. Only the C-C interaction cutoffs were increased up to the values which provide reasonable defect formation energies for the carbon self-interstitial in diamond. At a low substrate temperature (100 K), more than 10^3 carbon atom impacts were simulated, so that the steady-state growth mode of the films was achieved. In the simulated films, the surface region, the transition region to the substrate, and the inner region with nearly constant properties can be identified. The sp^3 fractions of the inner film regions lie between 52% and 95% for C^+ ion energies of $E_{ion}=30-80$ eV. The intrinsic stress and the elastic properties of these films were investigated in subsequent papers.[27–29] Altogether the approach reproduced essential trends of experimental data on diamondlike carbon.

Several analytic carbon potential functions[30–33] were described in the literature in 2000. Up to now one of these potentals was used in ta-C deposition simulations. Marks[30] developed it by extending upon an environment-dependent interaction potential (EDIP) proposed for silicon. Although the carbon EDIP does not account for π-bonding effects properly and treats all bonds between threefold sites as conjugated bonds in graphite, it incorporates long-range forces to model nonbonded π repulsion and, thereby, is free from the shortcomings of the Tersoff-Brenner-type potentials explained so far. The potential was used to investigate the amorphous networks generated by both liquid quenching[16,30] and beam deposition.[16,17] In the deposition simulations a rather low minimum ion energy is required to form ta-C. In particular, the film simulated with an energy of 3 eV and a substrate temperature of 20 °C possesses a sp^3 fraction of 50%. The growth process at 10 eV which is still entirely surface based provides even an sp^3-rich film ($\sim$55%). These results are not consistent with the phenomenological subplantation models.[5,6] Marks pointed out that the threshold energy for the transition from sp^2-rich to sp^3-rich material is difficult to measure; the reported values spread from 7 to 30 eV. He proposes[17] an alternative model of ta-C film growth in which ''energetic burial'' leads to the simultaneous processes of sp^3 promotion, densification, stress generation, and surface growth.

During the last years, we performed a series of further, very time-consuming MD deposition simulations, using the same model as in Ref. 14. Our aim was to check the approach more thoroughly under realistic process conditions, not only at a very low substrate temperature, but also at room temperature and at elevated temperatures. This allows for the effect of deposition temperature on relaxation processes during the film growth to be investigated. Films with a thickness of up to 10 nm were modeled, and the relaxation time after an ion impact was relatively long (15 ps). This paper summarizes the properties of all computed films. It is organized as follows. At first the model will be briefly explained, and one typical deposition simulation will be presented. Thereafter the bulk properties of the simulated films, i.e., sp^3 content, mass density, cohesive energy and intrinsic stress are described in dependence on ion energy and substrate temperature. In Sec. IV the average depth profiles of density and sp^3 fraction are discussed in more detail for the surface region. The simulations reveal the effect of substrate temperature on ta-C formation. This encouraged us to analyze the time scales characterizing the present MD approach (Sec. V). As a result, it will be demonstrated at the atomic level how the film formation process is influenced by deposition temperature.

II. MD DEPOSITION SIMULATIONS: METHOD AND EXEMPLIFICATION

The MD calculations were performed in the same manner as described elsewhere.[14] The evolution of the atoms in time and space is computed by the numerical solution of the clas-

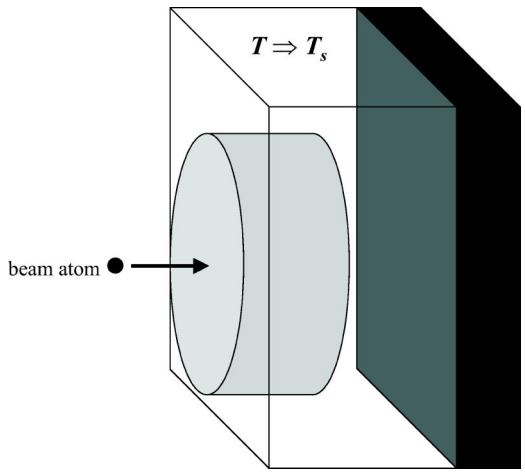

FIG. 1. Schematic representation of the proportions of our standard MD simulation cell (initial stage). The atoms inside the cylinder (radius $r=6.6$ Å) move exactly due to the interatomic potentials. The atoms within the white cuboid, but outside the cylinder, are coupled in addition to a heat bath of temperature T_s. The atoms within the bottom atomic layers (dark cuboid) have fixed positions. The deposition simulations started generally from a diamond {111} substrate consisting of 12 atomic layers with 56 C atoms per layer (for details, see Table I). In this case, the depth dimensions of the cylinder and of the white cuboid were 5.13 and 9.23 Å, respectively. In our large simulations with more than 3000 events, the number of the atoms having fixed positions is increased after every 56 events, so that the number of the active atoms remains nearly constant.

sical equations of motion. Brenner's analytic potential energy function (parameter set I of Ref. 20) is adopted, but with modified values $R=1.95$ Å and $S=2.25$ Å for the inner and outer cutoffs,[24] respectively. Successive impacts of up to 5000 energetic C atoms into diamond substrates with lateral dimensions of about 17.5×17.5 Å^2 are simulated. Periodic boundary conditions are used for the two directions perpendicular to the surface orientation. The bottom three atomic layers of the substrate (Fig. 1) are frozen. The atoms which are within a cylinder with a radius of 6.6 Å surrounding the initial direction of the incoming beam atom move strictly in accordance with the force field. The atoms outside the cylinder are coupled to a heat bath with the pre-defined temperature T_s of the substrate, employing the method of Berendsen *et al.*[34] The kinetic energies of these atoms are scaled after every integration time step dt by the factor

$$\lambda=\sqrt{1+\frac{dt}{\tau}\left(\frac{T_s}{T}-1\right)},$$

where T is the instant temperature of these atoms, and a value of $\tau=125$ fs is used for the relaxation time constant. In this manner, the kinetic energy brought in by the beam atom dissipates. In computing the initial stage of an impact we use time steps between 0.053 (for $E_{ion}=80$ eV) and 0.15 fs (for $E_{ion}=10$ eV). These values were then increased step by step depending on the actual maximum velocity. The atomic motions are followed for a relaxation time of 15 ps after every particle impact. The coordination of an atom is determined using the mean range $(R+S)/2=2.1$ Å of the potential as the cutoff length.

TABLE I. Ion beam deposition simulations analyzed in this paper. Shown are the process parameters (E_{ion}, T_s), the number of events, and the thickness of the inner film region with nearly constant properties. If not otherwise indicated, diamond {111} substrates consisting of 12 atomic layers with 56 C atoms per layer were used.

E_{ion} (eV)	Ion impacts	T_s (°C)	Film thickness (Å)
10	5000	20	74
20	5000	20	85
40 (two runs)	5000	20	64; 78
55 (two runs)	5000	20	65; 68
80	5000	20	61 [a]
40	3200	80	38 [b]
40	3200	130	39 [b]
40	5000	200	84
40	1200	400	9
40	1200	600	9
20	1200	-173	12 [c]
30	1200	-173	12 [c]
40 (three runs)	1200	-173	9 [c]; 12 [c]; 19
40	1200	-173	19 [d]
50	1200	-173	12 [c]
60	1200	-173	10 [c]
70	1200	-173	12 [c]
80	1200	-173	12 [c]

[a]Diamond {111} substrate with larger depth dimension (16 atomic layers).

[b]Diamond {111} substrate with larger depth dimension (22 atomic layers).

[c]Simulations presented already in Figs. 5 and 7 of Ref. 14.

[d]Diamond {001} substrate (14 atomic layers with 50 C atoms per layer).

The deposition simulations start from a diamond {111} substrate, except for one test run, where a diamond {001} substrate was used in order to verify the independence of the model predictions on substrate orientation. Table I informs in detail about the parameters of all simulations analyzed in this paper. The kinetic energy E_{ion} of the C^+ ion beams ranges up to 80 eV. Higher energies are not employed because of the increasing CPU time requirements. Shi *et al.*[35] concluded from investigations of ta-C films that there appear to be two different growth mechanisms before and after the peak sp^3 content at $E_{ion}\sim100$ eV. The present paper is restricted thus to the growth mechanisms before the peak. With regard to the substrate temperature T_s, our simulations can be separated into three groups: room temperature, high temperatures, and besides a rather low temperature (100 K) is included in order to investigate the maximum sp^3 content predicted for the given interatomic potential. For MD simulations, it is well known[12] that a decrease of the substrate temperature favors diamond-like properties.

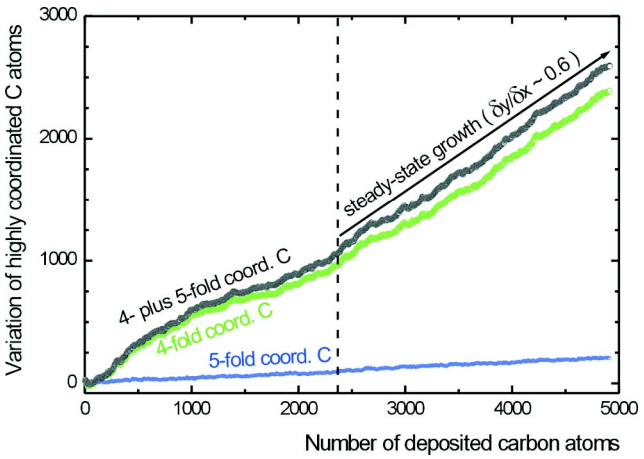

FIG. 2. Film growth by 40-eV C^+ ions implanted into a diamond {111} substrate at room temperature (first run; compare Table I). The variation of the number of fourfold and fivefold coordinated atoms in the MD supercell is plotted versus the number of deposited atoms. After the 5000 events, corresponding to a fluence of 1.6×10^{17} cm^{-2}, 4915 C atoms were deposited. 74 atoms, four C_2 molecules, and one C_3 molecule were sputtered. The CPU time for this simulation amounted to about 14 weeks.

Figures 2 and 3 depict a specific deposition simulation which is representative for this paper. 5000 impacts of 40 eV C^+ ions into a diamond substrate at room temperature were modeled. Figure 2 shows the increase in the number of fourfold coordinated C atoms versus the number of deposited

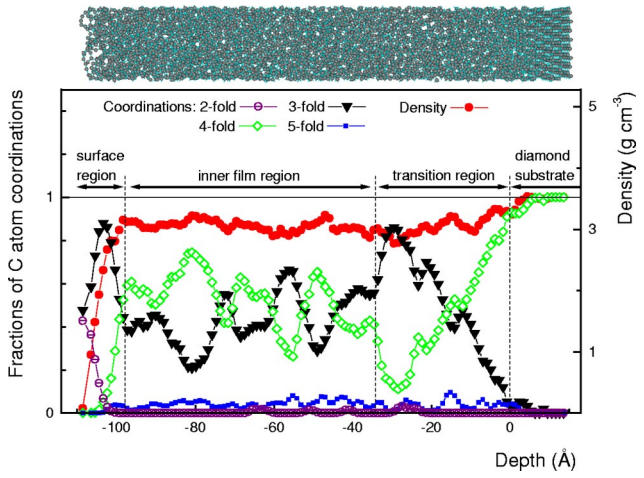

FIG. 3. Depth profiles of mass density (right-hand scale) and of all occurring atom coordinations (left-hand scale) in the film whose growth is illustrated in Fig. 2. The top part presents a snapshot of the atomic ensemble. In calculating the depth profiles, mass distributions of Gaussian shape having a width of 0.7 Å were used for the individual atoms. In addition, the profiles were averaged over intervals of 2.05 Å, corresponding to two atomic layers of the ideal diamond {111} substrate. This is the narrowest depth interval that can be used in order to obtain smooth profiles for the crystalline substrate. The substrate surface atoms were initially at the depth position $d=0$. Our quantitative partition into the three film regions, as indicated here, is somewhat arbitrary because of the large statistical fluctuations in the computed film properties.

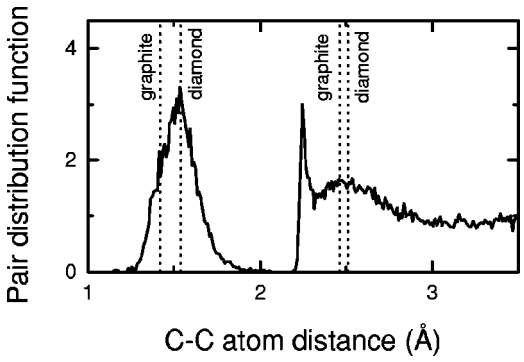

FIG. 4. Pair distribution function for the inner region of the 40-eV C^+ deposited film shown in Fig. 3. The vertical dotted lines mark first and second neighbor distances in graphite and diamond, respectively.

atoms. It demonstrates that more than 2000 impacts are necessary to attain the steady-state growth mode with the number of atoms of a specific coordination increasing linearly with the number of deposited atoms. Figure 3 shows the resultant film, and presents depth profiles across the film. The total film thickness is about 10 nm. One can distinguish three depth regions. The surface region, where the mass density raises from zero to its mean value, is dominated by threefold coordinated C atoms. This result is in good agreement with experimental investigations.[36] Some outermost atoms at the surface, however, exhibit twofold coordination. As expected in case of steady-state growth conditions, the film proves to have an inner region with nearly constant properties. Very large statistical fluctuations occur there, which might arise from the small lateral dimensions of the film. The last column of Table I lists the thickness of the inner film region for all deposition simulations covered in this paper.

The properties of the transition region between the film and the diamond substrate depend on substrate temperature T_s. At a very low temperature (100 K), the transition region lies inside the diamond surface region, is about 5 Å wide (Fig. 7 of Ref. 14), and for ion energies >40 eV there is a stress peak in this region.[28] The stress peak disappears at room temperature (see below), simultaneously the width of the transition region increases significantly. In the simulations performed for $T_s \geqslant 20$ °C, the transition region is about 20–30 Å broad, as shown in Fig. 3. According to the electron energy loss spectroscopy data of Davis *et al.*[36] the width of the transition region is about 20 Å for films deposited by 35 eV C^+ ions. Our value is in line with these data.

Typically 5% of the film atoms are predicted to remain in fivefold coordinated sites (see Ref. 14, and Figs. 2 and 3). Below (Sec. V) we shall give some arguments for the long term relaxation of these states to fourfold coordinated ones. In the remainder of this paper, the fractions of four- and fivefold coordinated atoms will be therefore sometimes added (as done in Fig. 2), and will then be interpreted as the sp^3 content of the simulated films.

Another disadvantage of the present approach becomes obvious if the pair distribution function of the atoms in the inner film region (Fig. 4) is considered. In the function, the

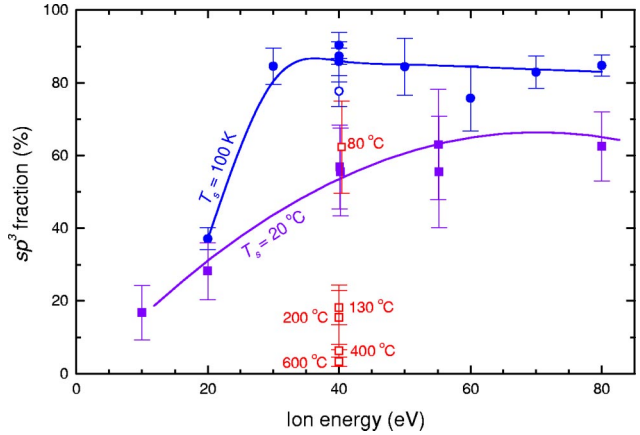

FIG. 5. Variation of sp^3 bonding in the simulated ta-C films as a function of C^+ ion energy E_{ion} and deposition temperature T_s. Different symbols are used in order to characterize orientation and temperature of the substrate: diamond {111} substrate and T_s = 100 K (●), 20 °C (■), 80–600 °C (□); and diamond {001} substrate, T_s = 100 K(○). The lines are included to guide the eye.

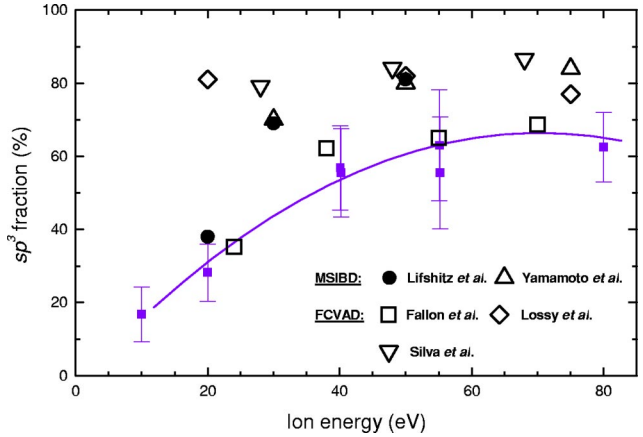

FIG. 6. Comparison of sp^3 fraction in the films simulated for T_s = 20 °C(■) with representative results of mass selected ion beam deposition (MSIBD) and filtered cathodic vacuum arc deposition (FCVAD). The data were taken from Lifshitz *et al.* (Ref. 38), Yamamoto *et al.* (Ref. 39), Fallon *et al.* (Ref. 40), Lossy *et al.* (Ref. 41), and Silva *et al.* (Ref. 42). For further measurements of sp^3 fractions, see Refs. 38 and 4.

position of the first neighbor peak coincides really with that of diamond, as expected in case of a dominant fraction of fourfold coordinated atoms (Fig. 3). However, an unexpected narrow peak occurs at the outer cutoff[24] value S = 2.25 Å. Such a spike is found for both the Tersoff[19] and Brenner[20] potentials, it is enhanced by the present enlargement of the cutoff parameters R and S (see Fig. 3 of Ref. 14). This problem was clarified by the recent investigations of Marks *et al.* Similar spikes were found there in amorphous carbon networks of high density produced by liquid quench[16] using the Brenner potential, and in a tight-binding simulation of film deposition,[37] where for reasons of computational efficiency the interaction was splined to zero at 2 Å. However, such spikes don't arise[16] if a variable cuttoff for C-C interactions is used (like in EDIP), or there is no interaction cuttoff (like in DF calculations). In particular, EDIP provides in this region a more realistic pair distribution function for the amorphous carbon networks generated by liquid quenching[16,30] or by deposition simulations.[17] In the Monte Carlo simulations of Kelires with the Tersoff potential such a very narrow spike was not found,[46] probably since the pair correlation function was averaged over thermal fluctuations at room temperature.

III. BULK PROPERTIES OF THE SIMULATED FILMS

In the following, the bulk properties of the simulated films (Table I) are analyzed. In Figs. 5, 6, and 7, sp^3 fractions and mass densities, which were averaged over the inner regions of the films, are presented together with their root mean square deviations (RMSDs). Figures 8 and 9 show the binding energy of the atoms inside the films. Compressive stress values are given in Figs. 10 and 11.

A. sp^3 bonding

The calculated sp^3 fractions are plotted vs ion energy and substrate temperature in Fig. 5. At a low substrate temperature (100 K), ta-C structures with a high sp^3 content of ~80% are modeled for beam energies $E_{ion} \geqslant 30$ eV. The simulated sp^3 content decreases with increasing substrate temperature. At room temperature, the sp^3 fractions are only in qualitative agreement with experimental data (Fig. 6). The upper values are too low, about 65% instead of the observed values of up to 80–90 %. In the present model, the formation of ta-C films results from an internal subsurface growth. The minimum energy which is required to deposit sp^3-rich films depends on temperature, it varies from ~25 eV at 100 K to ~35 eV at 20 °C.

For higher substrate temperatures, at E_{ion} = 40 eV, the model predicts a transition from an sp^3 content of (62.3

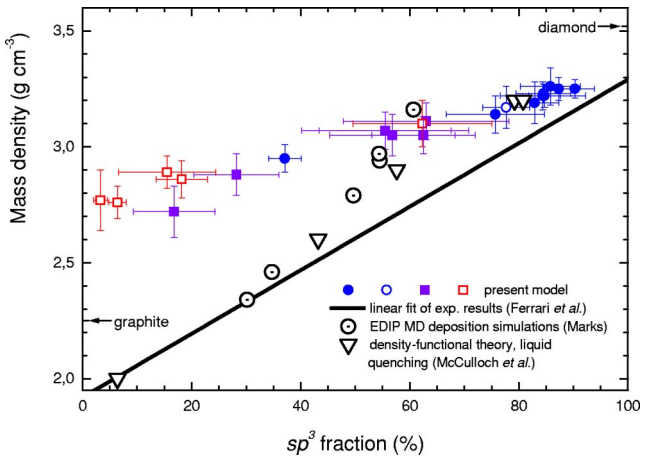

FIG. 7. Correlation of the density and sp^3 fraction for ta-C films. Our simulations (for the meaning of the different symbols, see Fig. 5) are compared to other theoretical predictions and to a linear fit of experimental results, derived by Ferrari *et al.* (Ref. 44) from their measurements and from the data of Fallon *et al.* (Ref. 40). The theoretical results included were taken from the EDIP deposition simulations of Marks (Ref. 17), and from the Car-Parrinello *ab initio* MD calculations performed for samples of 125 atoms by McCulloch *et al.* (Ref. 45).

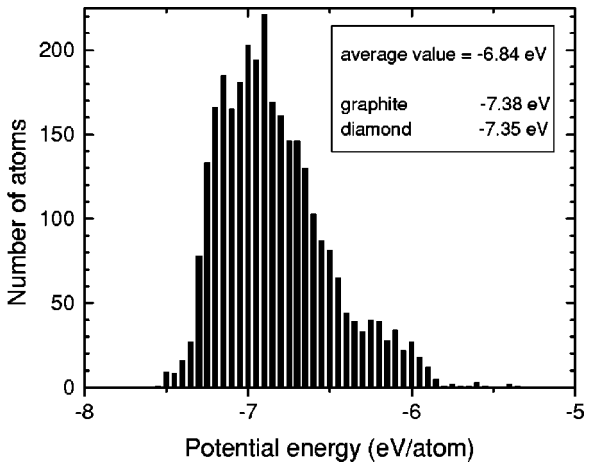

FIG. 8. Distribution of atomic energies in the bulk of the 40-eV C^+ deposited film shown in Fig. 3, after relaxing the film to a temperature of 0 K.

$\pm 12.7)\%$ at $T_s = 80$ °C to a value as low as $(18.2 \pm 4.6)\%$ at $T_s = 130$ °C (Fig. 5). This sharp transition is almost in agreement with reported data and may be considered as the most essential result of the present paper. In the experiments[1,43] the transition was found at somewhat higher temperatures, when T_s exceeds a critical temperature T_c of 150–200 °C. T_c decreases[43] with increasing ion energy E_{ion}, and equals 150 °C for 120 eV deposition.[1]

Because of the occurrence of the transition from sp^3-rich to sp^2-rich films, the deposition simulations for $T_s = 80$ and 130 °C were performed more carefully, with an increased number of active atoms (see footnote b of Table I). The differences between $T_s = 80$ and 130 °C will be analyzed and discussed in more detail below (Sec. V).

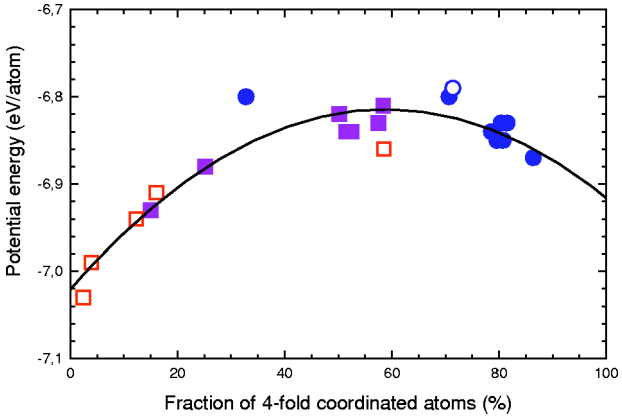

FIG. 9. Energetics predicted for the inner film regions. The average potential energy per bulk atom at a film temperature of 0 K is plotted vs the fraction of fourfold coordinated atoms; for the types of symbols, see Fig. 5. The solid line is the result of a polynomial fit of second order. The inner film regions contain threefold, fourfold, and fivefold coordinated atoms. The fractions of the fivefold coordinated atoms vary here between 0.8 and 6.3%, and the tendency is that this admixture increases with the fraction of fourfold coordinated atoms, i.e., with the *x*-axis values.

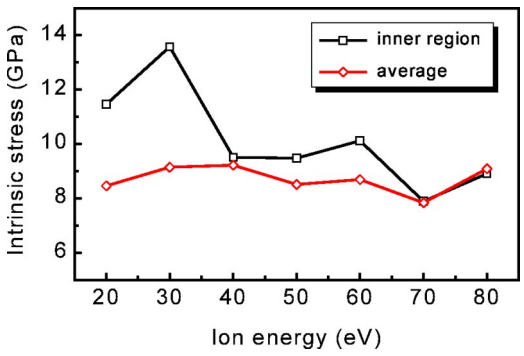

FIG. 10. In-plane intrinsic compressive stress at 0 K in amorphous carbon films deposited at a substrate temperature of 100 K vs ion energy. In calculating the average stress, the atomic level stresses were averaged either over the entire film or over the inner film region.

B. Mass density

Figure 7 shows the mass density of inner film regions as a function of the sp^3 content. Our density values refer to a film temperature of 20 °C. The films deposited at another temperature T_s were relaxed accordingly. In addition to the simulated results, Fig. 7 gives a linear function[44] representing a series of experimental measurements.[40,44] The results of the deposition simulations of Marks[17] and the predictions of a recent DF theory investigation[45] for amorphous carbon are also included.

The density values from the present simulations prove to follow a smooth line, even though large RMSDs occur. This demonstrates that all the present extensive calculations are compatible to each other. Our preceding paper[14] studied mainly films with a high sp^3 fraction of about 75–90 %. Now, in Fig. 7, the whole range of possible sp^3 fractions is covered by simulated films, and thereby the limitations of the present approach become more evident. The sp^3-rich ($>50\%$) amorphous C films obtained for $E_{ion} > 30$ eV, T_s

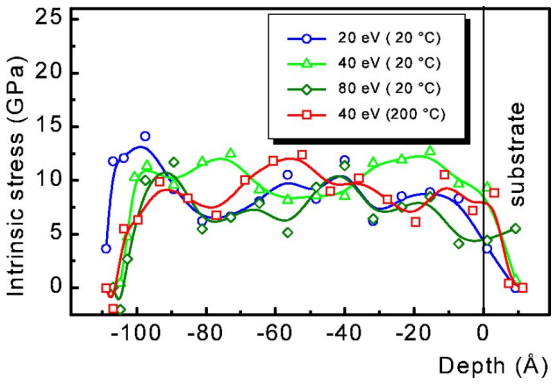

FIG. 11. Depth profiles of in-plane compressive stress at 0 K in amorphous carbon films deposited by ions of 20, 40, and 80 eV at $T_s = 20$ °C, and 40 eV at 200 °C. In calculating the depth profiles, the atomic-level stresses were averaged over layers of equal thickness of 8.2 Å, corresponding to eight atomic layers of an ideal (111) diamond substrate. The 40-eV, 20 °C results were taken from the film whose growth is illustrated in Fig. 2; for the final properties of this film, see Fig. 3.

$\leqslant$80 °C are modeled fairly well. We note that the maximum sp^3 content of about 65% calculated here for room temperature deposition coincides with the maximum sp^3 content in the EDIP deposition simulations of Marks.[17] But for graphite-like structures with a sp^3 fraction lower than 50%, our calculated densities are definitely too large. This is due to the absence of adequate long-range terms in Brenner's analytic potential energy function. Our increase of the interaction cutoff values is not sufficient to exclude threefold coordinated C structures which are more dense than graphite.[14] The inconsistency between density and high sp^2 content is generally a characteristic of potentials which do not properly describe nonbonded π repulsion. The deposition simulations of Marks provided sp^2-rich films ($\sim$65–70 % sp^2 fraction) for $E_{ion}=1$ eV and 2 eV. In these films, the relationship between density and coordination coincides with experimental data (Fig. 7) since two of the defining characteristics of EDIP are its treatment of non-bonded π repulsion and an appropriate interaction cutoff derived from DF theory calculations.[17]

C. Cohesive energy

The energetics of as-deposited ta-C films can be examined by analyzing calculated cohesive energies. Figure 8 shows a typical potential energy distribution of the bulk atoms in a film at 0 K. For the Tersoff-Brenner-type many-body potentials the partition

$$E_b = \sum_{i=1}^{N} E_i \tag{1}$$

of the binding energy E_b of the film into potential energies E_i of individual atoms (on-site energies) is not unique. In addition, the Brenner potential in its original form[20] gives the binding energy as a sum over bond energies rather than on-site energies. This difficulty can be overcome taking into account the symmetry $F_{CC}(i,j)=F_{CC}(j,i)$ of the correction function. Then E_b is represented[28] in the functional form of Tersoff[19] [Eq. (1)], with

$$E_i = \frac{1}{2}\sum_{j\neq i} \{V_R(r_{ij}) - b_{ij}V_A(r_{ij})\}, \tag{2}$$

and a new bond-order function $b_{ij}=B_{ij}+F_{CC}(i,j)/2$. This definition of on-site energies was shown[28] to result in a realistic distribution of the atomic-level stresses in amorphous carbon networks. The E_i distribution presented in Fig. 8 is very broad. Its average binding energy per atom is about 0.5 eV weaker than in graphite or diamond. The fivefold coordinated atoms possess a rather high energy of about -6.0 eV and thereby can be considered as interstitial defects in the amorphous carbon network. This provides an additional support for the on-site energy definition according to Eq. (2). Kelires obtained a similar distribution of atomic energies [see Fig. 3(a) of Ref. 46] when he modeled as-quenched ta-C cells, using a Monte Carlo approach and the Tersoff potential.[19]

Figure 9 illustrates the relationship between the average atomic energy and the fraction of fourfold coordinated atoms for all simulated films. The figure reveals that a film consisting of threefold coordinated atoms ($x=0$) is predicted to have a lower energy than films with $x>0$. The pure (100%) tetrahedral amorphous carbon is a less favorable state. Fitting the data by a polynomial of second order yields an energy curve which has a maximum near medium film composition. Accepting the fit in spite of its large statistical errors, the energy barrier separating a film of 85% sp^3 content from the more stable graphitic forms is about 0.04 eV. Although this low value, which corresponds to about 400 K, nicely correlates with the critical substrate temperature of $\sim$100 °C from the deposition simulations (Fig. 5), it does not entirely explain the dependence of subsurface film growth on T_s. The question arises why the thermal stability of the ta-C films against post-deposition annealing is significantly higher. During post-deposition thermal annealing in ultrahigh vacuum[47] an sp^3 content of 87% decreases only slightly up to 1100 °C. Thus, bulk ta-C must be separated from graphitic carbon by another barrier, being much higher than $\sim$0.04 eV. Recently we performed adequate MD annealing simulations[48] for ta-C, using the same empirical potential as in this paper, and reproduced the high thermal stability. The paradox between high graphitization temperature during annealing and low transition temperature in deposition is resolved by the nonlocal character of the sp^3 to sp^2 conversion, being represented by a collective reconstruction of an amorphous network involving many atoms. This can be easily achieved starting from a transient state with an ion of energy $E_{ion}\leqslant$80 eV being forced into the low density sp^2-rich surface layer (see below; Figs. 12 and 13), but not by heating already formed bulk ta-C.

D. Intrinsic stress

The origin of high intrinsic compressive stress, $\sigma\sim$10 GPa, in ta-C films and its role in ta-C formation appear to be the least understood aspects of the ta-C film growth process. It was initially proposed[8] that the high film stress induces a transition from graphitic a-C to ta-C, like high pressure induces a phase transition from graphite to diamond in crystalline carbon. This analogy was supported by an observation[49] that the diffuse transition region between ta-C and graphitic C in the (σ,T_s) plane is close to the Berman-Simon line separating diamond and graphite in the (P,T) phase diagram of carbon. However, recent experimental data[50] are contradictory to this hypothesis. Both ta-C films[51] (sp^3 fraction $\sim$80%) with comparatively low stress of $\sim$2 GPa and predominantly sp^2-bonded structures[52] with high stress of $\sim$12 GPa have been deposited. Therefore, the level of intrinsic stresses is not directly related to the sp^3 content in amorphous carbon films. It rather depends on the nature of relaxation processes during film growth. Some experimental data show[43] that the stress is correlated to density: below T_c it remains almost independent on T_s, whereas at T_c it falls abruptly. Such correlation between density and stress is covered by the ''subplantation models,''[6,53] which describe the relaxation of density and stress in terms of diffusion of the

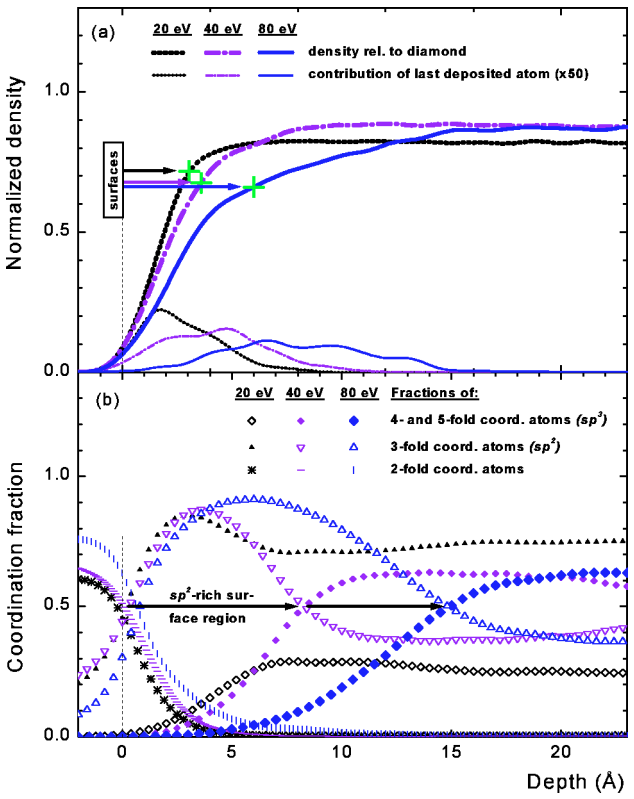

FIG. 12. Steady-state surface properties of films deposited with energies $E_{ion}=20$, 40, and 80 eV and at a substrate temperature $T_s=20$ °C. Depth profiles are shown (a) for the mass density relative to diamond and the contribution of the last deposited atom, which corresponds to a fluence of 3.3×10^{13} cm^{-2} into our simulation cell, and (b) for the fractions of differently coordinated atoms. All profiles were calculated by averaging over 150 subsequent film states, which were separated by 10 atom impacts, respectively, and were passed during the final stage of the deposition process under steady-state growth conditions. For a given atomic ensemble, Gaussian distributions of 0.7-Å standard deviation were used for the atoms; the depth value 0 was fixed to the position of the outermost surface atom. The 40-eV results were calculated for the film illustrated in Figs. 2 and 3.

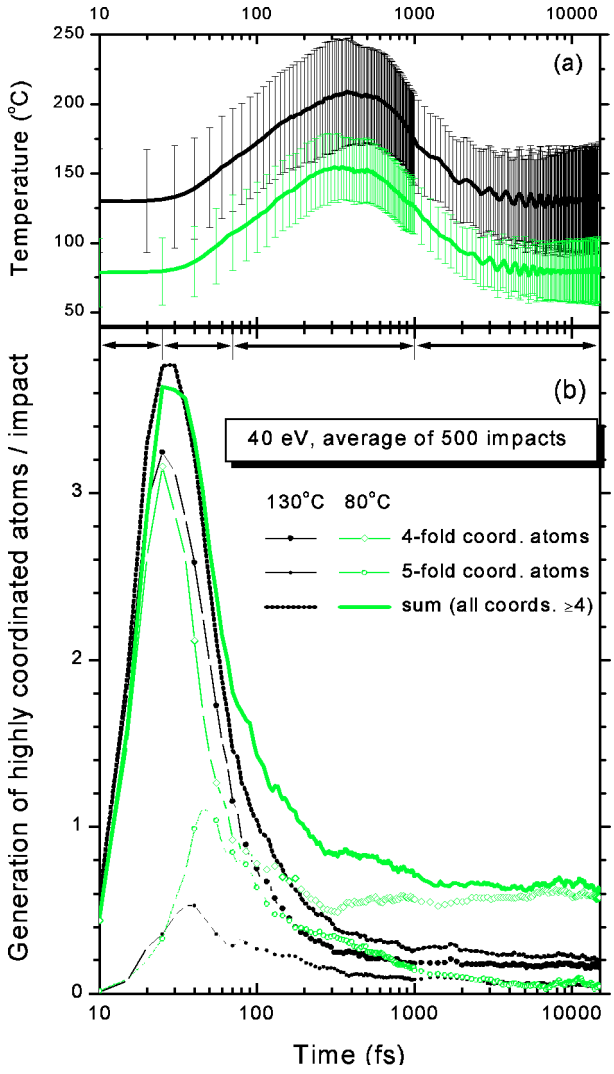

FIG. 13. The formation of highly coordinated atoms after a 40-eV C^+ ion impact, shown for the two substrate temperatures $T_s=80$ and 130 °C being just below and above the critical temperature for ta-C film simulation (compare Fig. 5). The figure presents (a) the temperature of the atoms coupled to the heat bath and (b) the increase in the number of four- and fivefold coordinated atoms as a function of time. The quantities were calculated by averaging over 500 successive events during steady-state film growth. The horizontal arrows mark time periods as discussed in the text.

excess atoms to the surface. On the other hand, low-temperature annealing experiments[47,54] clearly indicate an additional contribution of diffusionless mechanisms of stress relaxation. In principle, depending on deposition conditions, both diffusion-driven and diffusionless structural transformations in amorphous carbon networks may take place simultaneously. Figure 10 shows the level of intrinsic compressive stress in the films deposited at 100 K with different ion energies. The stress was calculated at $T=0$ K by averaging atomic level stresses[28] either over the entire film or only over the inner region. According to Ref. 28, at ion energies exceeding 40 eV there is a stress peak in the transition region between an amorphous carbon film and a diamond substrate. This peak compensates a low stress in the surface layer and therefore the average film stress and the stress in the inner film region coincide. Depth profiles of the zero temperature intrinsic stress in films deposited at $T_s=20$ °C with ion energies of 20, 40 and 80 eV are depicted in Fig. 11. The stress only slightly decreases as compared to Fig. 10, in accordance with experimental data.[43] The increase in substrate temperature from 100 K to 20°C eliminates the stress peak[28] at the substrate interface which is typical of low-temperature deposition at $E>40$ eV. Figure 11 also presents the stress profile in a film deposited with an ion energy of 40 eV at 200 °C, that is above T_c. In the deposition simulations with $E_{ion}=40$ eV the average film stress at $T_s=20$ and 200 °C is of 10.0 and 8.2 GPa, respectively, whereas in the experiment a stress reduction of $\sim$50% was observed.[43] The stress reduction, however, exactly follows the density reduction. This is in agreement with experiment. The smaller values for the stress reduction in the simulations as compared with experiment are due to the fact that the Brenner potential neglects

both the long-range repulsion of π orbitals and van der Waals attraction, thus overestimating the density of predominantly sp^2-bonded structures.

IV. FILM SURFACE

Figure 12 presents steady-state depth profiles in the surface region of films deposited with $E_{ion}=20$, 40, and 80 eV at room temperature. The profiles were calculated by averaging over 150 different surfaces; a Gaussian distribution of 0.7-Å standard deviation was used to describe the mass distributions of the single atoms. At the atomic scale, the surface of simulated amorphous carbon is not perfectly smooth. Rings of twofold coordinated C atoms stick out, and crater-shaped pits exist. Figure 3 shows an example. Under the twofold coordinated atoms, an sp^2-rich layer follows in any film [Fig. 12(b)]. For 80 eV, the sp^2-rich surface region is computed to extend to a depth of $\sim$15 Å. In the depth interval between 4 and about 15 Å a nearly constant rise of this density profile is found, which results from the continuously increasing sp^3 admixture.

The definition of a surface roughness for the simulated films is somewhat problematic. A reasonable assumption is that the surface reaches down to that depth where the fraction of threefold coordinated atoms peaks. At this depth, the decreasing fraction of twofold coordinated atoms and the increasing fraction of four-fold and fivefold coordinated atoms are just equal to each other. Accepting this definition, which is marked in Fig. 12(a) by horizontal arrows, surface roughness values can be evaluated by integrating the mass density profiles. The surface roughness derived in this way is predicted to increase with ion energy, and its root mean square (rms) values are 1.0, 1.4 and 2.8 Å for $E_{ion}=20$, 40, and 80 eV, respectively.

In the strict sense, these results are lower limits for the MD roughness, more correctly computed values might be larger, in view of the small lateral dimensions of the simulation cell. Calculating the roughness of phase boundaries by MD requires generally a sufficiently large cell, otherwise the result is limited by the cell dimensions.[55]

The surface morphology of ta-C films was studied by some groups. Roughness values were evaluated by averaging across much larger areas of typically 1×1 μm^2. Arena *et al.*[56] investigated films with a thickness of about 30 nm, produced by a filtered cathodic vacuum arc (FCVA) system, and showed that ta-C films deposited on Si has an rms surface roughness of 1.3 Å, increasing to about 10 Å for films deposited on metals such as Ti. Lifshitz *et al.*[57] deposited films $\sim$100 nm thick onto Si substrates using a mass selected ion beam source. The films retained the initial rms roughness of about 2 Å of the Si substrate over a wide energy region 30 eV$\leqslant E_{ion}\leqslant$10 keV. For $E_{ion}<30$ eV, when graphitic films evolve, the roughness increases with decreasing C^+ energy, and is about 10 Å for 20 eV. More recent investigations[35] of FCVA deposited, 60-nm-thick films on Si show that the smoothest films are formed at approximately 100 eV and have the highest sp^3 content. The rms roughness was reported to decrease from $\sim$4.5 Å at 75% sp^3 content to $\sim$1.2 Å at 88%. Other ta-C films prepared by Tang *et al.*[58] with mass selected 100-eV C^+ ions onto silicon had an rms roughness of $\sim$4 Å.

Comparing the present simulated data to the experimental findings, the roughness of the film with about 60% sp^3 content simulated for 80 eV is consistent with experiment. But there is clear disagreement for the dependence on ion energy. The spacious sp^2-rich film obtained for 20 eV is definitively too smooth. Rather than attributing this result to the small dimensions of the MD cell or to the start of the deposition simulations from an ideally smooth diamond substrate, we suspect that it is again caused by the absence of non-bonded long-range interactions in Brenner's potential, as for the film density (see above).

Figure 12(a) presents also the contributions of the last deposited atom to the film density. Such ion range profiles, but with a depth scale in units of at/cm^2, have been measured[59] by implanting ^{13}C ions into ^{12}C films and utilizing high-resolution elastic recoil detection. The comparison with the present MD simulations which will be reported in detail elsewhere[60] confirms the nonsymmetric shape of the profiles as shown in Fig. 12(a). The straggling of the calculated profiles however proves to be narrower than in measurements for energies up to $E_{ion}\sim$50 eV. This discrepancy can be explained by the present finding that the surface of the simulated films is too smooth. An increased surface roughness would really induce some broadening of the very shallow range profiles.

V. DISCUSSION: TIME-RESOLVED DYNAMICS OF THE FILM FORMATION

As stated above, the calculated critical temperature for ta-C film formation by 40-eV C^+ ions is about 100 °C. Therefore, in the following discussion we can focus on the two deposition simulations performed for 40 eV at substrate temperatures T_s of 80 and 130 °C (Table I), which provide sp^3 contents of 62% and 18%, respectively (Fig. 5). For a series of successive atom impacts the movement of the atoms in these two simulation runs was recorded in great detail, every 5 fs for the relaxation times up to 1 ps, and every 50 fs for the other relaxation periods (1–15 ps). Figure 13 presents, as a function of time and averaged over 500 events, the increase in the number of highly coordinated atoms. In addition, the instant temperature of the atoms coupled to the heat bath is plotted. Zero time is defined by the moment when the depth difference between the incident atom and the top surface atom is equal to the outer cutoff[24] $S=2.25$ Å of the potential.

First the evolution of temperature is considered. Because of the small dimensions of the simulation cell, we did not introduce local temperatures (for such data, see Ref. 61). The system is characterized by only one value. The incoming beam atom interacts first with target atoms which move exactly due to the interatomic forcefield. These are the atoms situated inside a cylinder surrounding the ''ion track,'' as illustrated in Fig. 1. The temperature given in Fig. 13(a) was derived from the kinetic energies of the other active atoms, outside the cylinder. Due to the energy flux out of the impact zone, this temperature begins to rise after 30 fs, on average.

The peak temperature occurs after ~400 fs. In case of dissipating the 40-eV incident energy to the kinetic and potential energies of all active atoms (about 1000), a maximum temperature increase by 0.02 eV or 200 °C would be expected. However, because of permanent cooling the actual rise in temperature is only ~80 °C. The system cools again down to the substrate temperature T_s in typically 5 ps. The effective cooling rate, which is determined by the cell dimensions and by the value of $\tau = 125$ fs used for the time constant in the Berendsen method (Sec. II), proves to be significantly slower than the cooling rates used in liquid quench MD techniques[62] to produce and investigate amorphous carbon. After thermalization, fluctuations in the temperature of the system may appear if temperature-driven relaxation processes consume or release kinetic energy.

Concerning the theoretical temperatures presented throughout this paper, there is a fundamental problem which has to be mentioned here. In calculating the instant temperature values, the average kinetic energy per carbon atom is divided by $\frac{3}{2}k$ in accordance with the equipartition theorem. This relationship of the classical statistical mechanics is commonly used in MD studies of amorphous carbon.[61,62] But the subjects are diamondlike materials, and diamond is the crystal with the highest Debye temperature (2220 K). Its heat capacity at room temperature is about 4 times smaller than the high-temperature classical limit. The Brenner potential used throughout this paper (parameter set I of Ref. 20) makes tetrahedrally coordinated C structures more classical. It underestimates[27] the elastic constants of diamond and consequently also its Debye temperature. For ta-C, the potential provides elastic constants[29] which would lead to a Debye temperature of ~1200 K. Even this value is too high for quantum effects to be neglected.

The problem of matching better theoretical temperature values is not very important for the analysis of ta-C film properties as done in the preceding sections, since both the measured and the simulated properties vary only slightly with T_s below the transition temperature. But the computed value of T_c becomes questionable. The fact that a too low transition temperature was obtained (Sec. III A) appears to be due to the net effect of an inappropriately ''soft'' potential and the classical statistics.

The presentation in Fig. 13(b) provides information on the chronological order of the film formation processes. The average net generation of highly coordinated atoms per C^+ impact is plotted versus time in order to reveal how far the hitherto existing ideas can be substantiated by atomistic simulations. To simplify the explanation of the specific curves ($E_{ion} = 40$ eV), four stretches of time are marked, instead of the three time scales used in the literature. Let us elucidate these periods:

A. Subplantation ($t = 0 - 25$ fs)

The curves reflect the increasing number of atoms in the first neighbors sphere of the projectile when it is entering the target. The recoils begin just to move, changes in their bonds to target atoms do not dominate yet the plot. If the incident atom is forced between three atoms being before 1× twofold and 2× threefold coordinated ones, then three new highly coordinated atoms are generated. The peaks of the curves at 25 fs are somewhat higher than 3, since there are contributions where the twofold coordinated atom mentioned is replaced by a higher coordinated atom. In the course of these 25 fs the projectile loses half of its kinetic energy, on average.

B. Stopping and temperature-independent relaxations ($t = 25 - 70$ fs)

The incident atom comes almost to rest during this period, it is decelerated to an energy of about 1 eV. The maximum kinetic energy of any atom in the system is ~2 eV. The instant temperature of the atoms coupled to the heat bath begins to rise. The system relaxes to a certain energy minimum and the coordinations of all slowed down collision cascade atoms are significantly controlled by the potential energy landscape. Only in this way one can explain that the total production of highly coordinated atoms per incidence decreases and reaches values near unity. An ultimate value of unity would be realized in case of steady-state growth of a purely sp^3-bonded film. In our example, the average values at 70 fs amount to 1.8 and 1.5 new highly coordinated atoms for substrate temperatures of 80 and 130 °C, respectively. In a first approximation, these two values can be considered to be equal to each other, and thus to be independent on temperature. But their respective separation into new four- and fivefold coordinated atoms depends on T_s, since the two targets are films already grown at $T_s = 80$ °C and 130 °C.

C. Temperature-dependent relaxation ($t = 70 - 1000$ fs)

At the beginning of this period the simulation cell temperature continues to rise. The maximum value is achieved after ~360 fs, thereafter the temperature decreases. The film relaxation is now governed by temperature. For our higher substrate temperature ($T_s = 130$ °C), the numbers of new four- and fivefold coordinated atoms decrease continuously, and at $t = 1000$ fs a total fraction of only 0.26 new highly coordinated atoms exists per event. For the lower substrate temperature ($T_s = 80$ °C), the number of new fivefold coordinated atoms decreases too, even to a larger degree. But for $t > 300$ fs, an essential part of the vanishing fivefold coordinated atoms relaxes to fourfold coordinated ones, and thus the fraction of new fourfold coordinated atoms increases again. This behavior is a *ex post facto* justification of our former assumption (see above and Ref. 14) to interpret four- plus fivefold coordinated atoms as sp^3 content of the films.

D. Temperature-driven stabilization ($t > 1$ ps)

For times $t > 1$ ps the relaxation processes continue and act in a similar way. Because of the falling cell temperatures, bond breaks or formations happen less frequently. For longer times (~9–15 ps), before the next beam atom impinges on the sample, statistical fluctuations begin to dominate all curves plotted in Fig. 13, the averaged derivatives are nearly zero. Thus, our total relaxation time of 15 ps appears to be sufficiently large to understand the essentials of ta-C film formation.

Figure 13 reveals an additional reason for the theoretical critical temperature of ~100 °C for 40 eV to be smaller than in experiments. In the period when the most important temperature-dependent relaxation processes are predicted to be realized ($t=70-1000$ fs), the temperature of the coupled to the heat bath part of the simulation cell exceeds the pregiven substrate temperature T_s. The corresponding overheating of 30–80 °C diminishes the temperature gradient in the whole cell, reducing the energy flux out of the impact zone. A more accurate estimate for T_c would require larger lateral MD cell dimensions to ensure better description of thermostatting.

The time scales of the physical processes involved in ta-C film formation were estimated more than one decade ago, when the ideas of subplantation have been established. According to Lifshitz and co-workers,[5,63,64] the three time scales[65] characterizing the evolution of the film can be described as follows: (i) a collisional stage, in which the projectiles transfer their kinetic energy to the target atoms (100 fs); (ii) a thermalization stage, in which the energetic atoms participating in the collision cascade dissipate their excess energy to lattice (less than 10 ps); (iii) a long-term relaxation stage (more than 100 ps), in which the final structure of the material is determined. The second stage, which is poorly understood, is often discussed in ''thermal spike'' notations. The third stage is assumed to be governed by thermally activated processes such as diffusion of interstitials and vacancies, phase transformations and chemical reactions.[64]

Figure 13 shows that the atomistic simulations provide similar time intervals for the collisional regime and for thermalization of the cascade region. Interesting results are the high degree of structure relaxation during the initial collisional regime, and the extensive formation of the final temperature-dependent film properties at times as small as ~1 ps. For the relaxation during the collisional and thermalization stages, the many-body effects are predicted to be more important than it was previously expected. Furthermore, the film relaxation seems to end in Fig. 13 after ~10 ps. This interpretation, which would disclaim the importance of long-term relaxations, is too crude. Apart from the much longer time being available under realistic conditions between the events, the curves plotted in Fig. 13 are averaged over many ion impacts. In our simulations, we had about 1000 active atoms and a time interval of 15 ps between the successive impacts. Consequently, the movement of individual atoms was considered for ~15 ns. Figure 13 indicates that all the long-term relaxations taking place during the 15 ns are induced by the action of a subsequent incoming ion (ion-assisted relaxation). A more definite investigation of the problem would require a spatial-resolved analysis which is beyond the scope of this paper.

Finally, one can relate Fig. 13 to the other results of this paper. In doing so, the ta-C film formation predicted by the present model can be characterized as follows: Forcing carbon ions with $E_{ion}=30-80$ eV under steady-state growth conditions into the appropriate film, the incidence particles come to rest, with a very high probability, in the sp^2-rich surface layer (Fig. 12). The subplantation into a threefold coordinated region generates initially, in any case, a few fourfold coordinated sites [Fig. 13(b), $t<70$ fs], and after relaxation nearly one new fourfold coordinated site per subplanted atom remains, on average. Due to the concurrent densification of the corresponding region, this process doesn't necessarily require a subsequent long-term relaxation, such as outdiffusion of an excess atom. The relaxation process will be more complex if the incidence atom, or the recoils, come to rest in fourfold coordinated areas. Then fivefold coordinated sites are primarily generated too, and mass transport out of these areas is necessary to maintain density and coordination type.

The network of highly coordinated atoms induced by subplantation is in a metastable state (Fig. 9). For supercritical substrate temperatures ($T_s>T_c$), the kinetic energy of the atoms is high enough to overcome the barrier in cohesive energy between diamondlike and graphitelike films. As a result, the relaxation processes lead finally to the more stable graphitelike amorphous network. For subcritical substrate temperatures ($T_s<T_c$) the diamondlike film is stable.

VI. CONCLUSIONS

Using an analytic interatomic potential of Brenner with an increased C-C interaction range, ion beam deposition of amorphous carbon films was simulated. The model correctly describes the properties of highly tetrahedral (ta-C) films, while density and roughness of sp^2-rich graphitic films are not properly reproduced. The main reason is that the potential doesn't account for the long-range repulsion between π orbitals.

In the present simulations, the process of ta-C formation from C^+ ion beams has an essentially subsurface nature and depends critically on both ion energy and substrate temperature. In contrast to Ref. 17 and in agreement with the phenomenological subplantation models,[1,5,6] no amorphous carbon films with diamondlike properties were deposited at ion energies of less than 20 eV. The incorporation of incoming ions into subsurface layers is not by itself sufficient to produce ta-C. For successful ta-C film deposition the relaxation processes leading to the sp^3 to sp^2 conversion have to be suppressed. The simulations clearly show that a transition from ta-C to graphitic carbon occurs within a narrow temperature range of ~50 °C, confirming the experimentally observed sharp dependence of the sp^3 content on substrate temperature. An essential finding of this study is that at the time scale of about 0.5 ps the relaxation processes in growing films below and after T_c proceed differently, leading in the first case to highly tetrahedral and in the second case to graphitic amorphous carbon films.

ACKNOWLEDGMENTS

We gratefully acknowledge financial support by the Deutsche Forschungsgemeinschaft. For the many helpful discussions, we would like to thank Professor W. Möller, Dr. W. Bürger, Dr. K.-H. Heinig, Dr. M. Posselt, and Dr. B. Schultrich.

*Electronic address: H.U.Jaeger@fz-rossendorf.de
†Permanent address: Institute of Crystallography, Russian Academy of Sciences, Moscow, Russia.

[1] Y. Lifshitz, Diamond Relat. Mater. **8**, 1659 (1999), and references therein.
[2] W.I. Milne, A. Ilie, J.B. Cui, A. Ferrari, and J. Robertson, Diamond Relat. Mater. **10**, 260 (2001).
[3] J. Robertson, Thin Solid Films **383**, 81 (2001).
[4] H. Hofsäss, H. Feldermann, R. Merk, M. Sebastian, and C. Ronning, Appl. Phys. A: Mater. Sci. Process. **66**, 153 (1998), and references cited therein in Section II.
[5] Y. Lifshitz, S.R. Kasi, and J.W. Rabalais, Phys. Rev. Lett. **62**, 1290 (1989).
[6] J. Robertson, Diamond Relat. Mater. **2**, 984 (1993).
[7] B.A. Pailthorpe, J. Appl. Phys. **70**, 543 (1991).
[8] D.R. McKenzie, D. Muller, and B.A. Pailthorpe, Phys. Rev. Lett. **67**, 773 (1991).
[9] N.A. Marks, D.R. McKenzie, and B.A. Pailthorpe, Phys. Rev. B **53**, 4117 (1996).
[10] S. Uhlmann, Th. Frauenheim, and Y. Lifshitz, Phys. Rev. Lett. **81**, 641 (1998).
[11] H.-P. Kaukonen and R.M. Nieminen, Phys. Rev. Lett. **68**, 620 (1992).
[12] M.O. Kaukonen and R.M. Nieminen, Surf. Sci. **331-333**, 975 (1995).
[13] M. Kaukonen and R.M. Nieminen, Phys. Rev. B **61**, 2806 (2000).
[14] H.U. Jäger and K. Albe, J. Appl. Phys. **88**, 1129 (2000).
[15] S. Yastrebov and R. Smith, Phys. Rev. B **180**, 145 (2001).
[16] N.A. Marks, N.C. Cooper, D.R. McKenzie, D.G. McCulloch, P. Bath, and S.P. Russo, Phys. Rev. B **65**, 075411 (2002).
[17] N. Marks, J. Phys.: Condens. Matter **14**, 2901 (2002).
[18] G.C. Abell, Phys. Rev. B **31**, 6184 (1985).
[19] J. Tersoff, Phys. Rev. B **39**, 5566 (1989); **41**, 3248 (1990).
[20] D.W. Brenner, Phys. Rev. B **42**, 9458 (1990); **46**, 1948 (1992).
[21] B. Weiner, S. Skokov, and M. Frenklach, J. Chem. Phys. **102**, 5486 (1995).
[22] P. de Sainte Claire, K. Song, W.L. Hase, and D.W. Brenner, J. Phys. Chem. **100**, 1761 (1996).
[23] J. Furthmüller, J. Hafner, and G. Kresse, Phys. Rev. B **53**, 7334 (1996).
[24] Tersoff as well as Brenner used in their formulas for the pair interactions a cutoff function simply taken as (see Refs. 19 and 20)

$$f_C(r)=\begin{cases}1, & r<R\\ \frac{1}{2}+\frac{1}{2}\cos\left[\frac{\pi(r-R)}{S-R}\right], & R\leqslant r\leqslant S,\\ 0, & r>S\end{cases}$$

which has continuous value and derivative for all bond lengths r, and goes from 1 to 0 in a small range around $(R+S)/2$.
[25] K. Nordlund, J. Keinonen, and T. Mattila, Phys. Rev. Lett. **77**, 699 (1996).
[26] R. Smith and K. Beardmore, Thin Solid Films **272**, 255 (1996).
[27] A.Yu. Belov and H.U. Jäger, in *Growth, Evolution and Properties of Surfaces, Thin Films and Self-Organized Structures*, edited by S.C. Moss, MRS Symposia Proceedings No. 648 (Materials Research Society, Pittsburgh, 2001), p. P6.53.
[28] A.Yu. Belov and H.U. Jäger, Comput. Mater. Sci. **24**, 154 (2002).
[29] A.Yu. Belov and H.U. Jäger, Surf. Coat. Technol. **151-152**, 128 (2002).
[30] N.A. Marks, Phys. Rev. B **63**, 035401 (2000).
[31] D.G. Pettifor and I.I. Oleinik, Phys. Rev. Lett. **84**, 4124 (2000).
[32] D.W. Brenner, Phys. Status Solidi B **217**, 23 (2000).
[33] S.J. Stuart, A.B. Tutein, and J.A. Harrison, J. Chem. Phys. **112**, 6472 (2000).
[34] H.J.C. Berendsen, J.P.M. Postma, W.F. van Gunsteren, A. DiNola, and H.R. Haak, J. Chem. Phys. **81**, 3684 (1984).
[35] X. Shi, L.K. Cheah, J.R. Shi, Z. Sun, and B.K. Tay, J. Phys.: Condens. Matter **11**, 185 (1999).
[36] C.A. Davis, G.A.J. Amaratunga, and K.M. Knowles, Phys. Rev. Lett. **80**, 3280 (1998).
[37] N.C. Cooper, M.S. Fagan, C.M. Goringe, N. Marks, and D.R. McKenzie, J. Phys.: Condens. Matter **14**, 723 (2002).
[38] Y. Lifshitz, Diamond Relat. Mater. **5**, 388 (1996).
[39] K. Yamamoto, T. Watanabe, K. Wazumi, F. Kokai, Y. Koga, and S. Fujiwara, Diamond Relat. Mater. **10**, 895 (2001).
[40] P.J. Fallon, V.S. Veerasamy, C.A. Davis, J. Robertson, G.A.J. Amaratunga, W.I. Milne, and J. Koskinen, Phys. Rev. B **48**, 4777 (1993); **49**, 2287(E) (1993).
[41] R. Lossy, D.L. Pappas, R.A. Roy, J.P. Doyle, J.J. Cuomo, and J. Bruely, J. Appl. Phys. **77**, 4750 (1995).
[42] S.R.P. Silva, S. Xu, B.X. Tay, H.S. Tan, and W.I. Milne, Appl. Phys. Lett. **69**, 491 (1996).
[43] M. Chhowalla, J. Robertson, C.W. Chen, S.R.P. Silva, C.A. Davis, G.A.J. Amaratunga, and W.I. Milne, J. Appl. Phys. **81**, 139 (1997).
[44] A.C. Ferrari, A. Libassi, B.K. Tanner, V. Stolojan, J. Yuan, L.M. Brown, S.E. Rodil, B. Kleinsorge, and J. Robertson, Phys. Rev. B **62**, 11089 (2000).
[45] D.G. McCulloch, D.R. McKenzie, and C.M. Goringe, Phys. Rev. B **61**, 2349 (2000).
[46] P.C. Kelires, Phys. Rev. B **47**, 1829 (1993).
[47] A.C. Ferrari, B. Kleinsorge, N.A. Morrison, A. Hart, V. Stolojan, and J. Robertson, J. Appl. Phys. **85**, 7191 (1999).
[48] A.Yu. Belov and H.U. Jäger, Nucl. Instrum. Methods Phys. Res. B **202**, 242 (2003).
[49] D.R. McKenzie, Y. Yin, N.A. Marks, C.A. Davis, B.A. Pailthorpe, G.A.J. Amaratunga, and V.S. Veerasamy, Diamond Relat. Mater. **3**, 353 (1994).
[50] A.C. Ferrari, S.E. Rodil, J. Robertson, and W.I. Milne, Diamond Relat. Mater. **11**, 994 (2002).
[51] M. Bonelli, A.C. Ferrari, A. Fioravanti, A. Li Bassi, A. Miotello, and P.M. Ossi, Eur. Phys. J. B **25**, 269 (2002).
[52] R.G. Lacerda, P. Hammer, C.M. Lepienski, F. Alvarez, and F.C. Marques, J. Vac. Sci. Technol. A **19**, 971 (2001).
[53] C.A. Davis, Thin Solid Films **226**, 30 (1993).
[54] T.A. Friedmann, J.P. Sullivan, J.A. Knapp, D.R. Tallant, D.M. Follstaedt, D.L. Medlin, and P.B. Mirkarimi, Appl. Phys. Lett. **71**, 3820 (1997).
[55] K. Gärtner and B. Weber, Nucl. Instrum. Methods Phys. Res. B **202**, 255 (2003).
[56] C. Arena, B. Kleinsorge, J. Robertson, W.I. Milne, and M.E. Welland, J. Appl. Phys. **85**, 1609 (1999).
[57] Y. Lifshitz, G.D. Lempert, and E. Grossman, Phys. Rev. Lett. **72**, 2753 (1994); E. Grossmann, G.D. Lempert, J. Kulik, D. Marton, J.W. Rabalais, and Y. Lifshitz, Appl. Phys. Lett. **68**, 1214 (1996).
[58] Z. Tang, Z.J. Zhang, K. Narumi, Y. Xu, H. Naramoto, S. Nagai,

and K. Miyashita, J. Appl. Phys. **89**, 1959 (2001).
[59] P. Neumaier, G. Dollinger, A. Bergmaier, I. Genchev, L. Görgens, R. Fischer, C. Ronning, and H. Hofsäss, Nucl. Instrum. Methods Phys. Res. B **183**, 48 (2001).
[60] P. Neumaier, G. Dollinger, A. Bergmaier, W. Eckstein, R. Fischer, L. Görgens, H. Hofsäss, H. U. Jäger, H. Kröger, and C. Ronning (unpublished).
[61] B.A. Pailthorpe, D. Mitchell, and N.S. Bordes, Thin Solid Films **332**, 109 (1998).
[62] N.A. Marks, Phys. Rev. B **56**, 2441 (1997).
[63] Y. Lifshitz, S.R. Kasi, J.W. Rabalais, and W. Eckstein, Phys. Rev. B **41**, 10468 (1990).
[64] Y. Lifshitz, G.D. Lempert, E. Grossmann, I. Avigal, C. Uzan-Saguy, R. Kalish, J. Kulik, D. Marton, and J.W. Rabalais, Diamond Relat. Mater. **4**, 318 (1995).
[65] B.W. Dodson, in *Processing and Characterization of Materials Using Ion Beams*, edited by L.E. Rehn, J. Greene, and F.A. Smidt, MRS Symposia Proceedings No. 128 (Materials Research Society, Pittsburgh, 1989), p. 137.